Effect of proton irradiation energy on SiN$_X$/AlGaN/GaN metal-insulator semiconductor high electron mobility transistors

Chaker Fares, Fan Ren, Stephen J. Pearton, Gwangseok Yang, Jihyun Kim, Chien-Fong Lo, and J. Wayne Johnson

Effect of proton irradiation energy on SiN$_x$/AlGaN/GaN metal-insulator semiconductor high electron mobility transistors

Chaker Fares,[1] Fan Ren,[1,a)] Stephen J. Pearton,[2] Gwangseok Yang,[3] Jihyun Kim,[3] Chien-Fong Lo,[4] and J. Wayne Johnson[4]

[1]Department of Chemical Engineering, University of Florida, Gainesville, Florida 32611
[2]Department of Materials Science and Engineering, University of Florida, Gainesville, Florida 32611
[3]Department of Chemical and Biological Engineering, Korea University, Seoul 136-713, South Korea
[4]IQE, Taunton, Massachusetts 02780

The effects of proton irradiation energy on the electrical properties of SiN$_x$/AlGaN/GaN metal-insulator semiconductor high electron mobility transistors (MISHEMTs) using *in situ* grown silicon nitride as the gate dielectric were studied. The SiN$_x$/AlGaN/GaN MISHEMT devices were irradiated with protons at energies of 5, 10, or 15 MeV at a fixed fluence of $2.5 \times 10^{14} \, \text{cm}^{-2}$. The largest amount of device degradation was shown in the samples irradiated with the lowest irradiation energy of 5 MeV. The DC saturation current was reduced by 10.4%, 3.2%, and 0.5% for MISHEMTs irradiated with proton energies of 5, 10, and 15 MeV, respectively. Device performance degradation was more pronounced in the irradiated samples under high-frequency operation. At a frequency of 100 kHz, the percent saturation drain current reduction at a gate voltage of 3 V was 40%, 19%, and 17% after proton irradiation at 5, 10, and 15 MeV, respectively. The carrier removal rates for the MISHEMT devices were in the range of 21–144 cm^{-1} for the proton irradiation energies studied. The measured DC degradation and carrier removal rates are lower than the values reported for AlGaN/GaN metal-gate high electron mobility transistor devices irradiated at similar conditions, which can be attributed to the SiN$_x$ insulating layer reducing the total damage on the AlGaN surface. *Published by the AVS.* https://doi.org/10.1116/1.5049596

I. INTRODUCTION

In applications such as satellite-based communication, remote sensing, radar technology, and nuclear energy production, radiation-hard microelectronics must be utilized. The primary cosmic ray flux, originating outside of the Earth's atmosphere, is composed mostly of protons (90%), so the effect of these ions on electronic devices that might be used in space-borne systems is of particular relevance. AlGaN/GaN high electron mobility transistors (HEMTs) are well suited to these applications because of their ability to operate under uncooled conditions and have shown a higher resistance to damage by irradiation with energetic ions than gallium arsenide- and silicon-based devices due to the high bond strength of binary/ternary nitrides and low defect formation rates.[1–9] Despite promising device characteristics, AlGaN/GaN-based HEMTs often suffer from high gate leakage and can be limited by dynamic behavior degradation caused by gate-lag trapping effects on the AlGaN surface.[10–15] To minimize gate leakage and enhance gate swing within HEMTs, dielectric insulators such as HfO$_2$, Al$_2$O$_3$, SiO$_2$, and SiN$_x$ have been utilized between the gate contacts and heterostructure interface. Based on several studies, these metal-insulator semiconductor high electron mobility transistors (MISHEMTs) have been shown to successfully reduce gate leakage and produce higher breakdown voltages than metal-gate devices.[16–19] Among these gate dielectrics, plasma enhanced chemical vapor deposition SiN$_x$ has been commonly used in AlGaN/GaN HEMTs to passivate surface trap states and mitigate gate-lag effects and drain current collapse.[20–24] The study of proton irradiation energy on device performance is important in developing radiation-tolerant systems.[25–28]

Several groups have reported on the effects of proton irradiation energy on conventional AlGaN/GaN HEMTs, AlGaN/GaN metal oxide semiconductor high electron mobility transistors (MOSHEMTs), and also InAlN/GaN HEMTs.[27,29–33] For InAlN/GaN HEMTs irradiated with protons at 5 MeV, a 72% reduction in saturation current was observed at a fluence of $5 \times 10^{15} \, \text{cm}^{-2}$, and at 15 MeV, a 66% reduction in drain current was observed using the same fluence.[34] Kim *et al.*[33] studied the degradation effects of proton irradiation energies ranging from 5 to 15 MeV on AlGaN/GaN HEMTs at a fixed fluence of $5 \times 10^{15} \, \text{cm}^{-2}$ and reported that devices irradiated at lower energies showed larger degrees of degradation. Ahn *et al.*[31] investigated the effects of proton irradiation energy on InAlN/GaN MOSHEMTs and reported a 2.5 times increase in sheet resistance for devices irradiated at 15 MeV, whereas a 10 times increase was observed in devices irradiated at 5 MeV. Hu *et al.*[25] investigated the proton induced degradation in AlGaN/GaN HEMTs at energies up to 105 MeV. They reported no significant degradation in the HEMTS irradiated with protons in the energy range of 15–105 MeV at fluences lower than $10^{11} \, \text{cm}^{-2}$. Despite a significant amount of data reported on the effects of proton irradiation energy on HEMTs and MOSHEMTs, information on proton radiation effects on SiN$_x$/AlGaN/GaN MISHEMTs is absent. It is worth investigating the performance of AlGaN/GaN
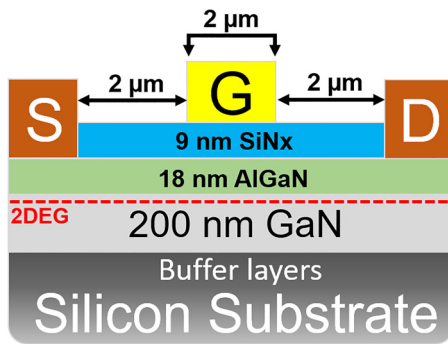
a)Electronic mail: fren@che.ufl.edu

FIG. 1. Device schematic of SiN$_x$/AlGaN/GaN MISHEMT used in this study.

MISHEMTs after proton induced damage to better understand the radiation hardness for space-based applications.

In this paper, we report the effects of different energy proton irradiation energies on drain and gate current–voltage characteristics, mobility, contact resistance, sheet resistance, subthreshold swing, and gate-pulsed characteristics of SiN$_x$/AlGaN/GaN MISHEMTs. The carrier removal rates of the proton irradiations were also determined.

II. EXPERIMENT

The AlGaN/GaN MISHEMT structure consisted of a 9 nm *in situ* SiN$_x$, an 18 nm AlGaN barrier layer, a 200 nm GaN channel layer, a 4200 nm GaN buffer layer, and a 180 nm AlN nucleation layer deposited on 8 in. Si substrates with a metal organic chemical vapor deposition system. For the fabrication of the MISHEMT devices, source and drain regions were created by the deposition of Ti/Al/Ni/Au Ohmic contacts which were annealed in flowing N$_2$ at 850 °C. To achieve interdevice isolation, nitrogen ion implantation was performed at various fluences and energies.[35] Electron beam deposited Ni/Au-based metallization was employed for 2 μm gate length Schottky gates. The device schematic and layer structure are illustrated in Fig. 1.

Proton irradiations were performed at the Korean Institute of Radiological & Medical Sciences using an MC 50 (Scanditronix) cyclotron. The proton energy at the exit of the
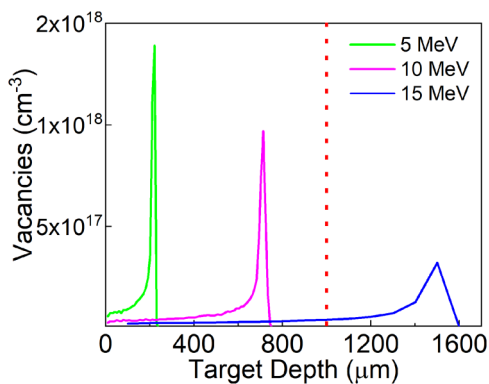
TABLE I. Sheet and contact resistances before and after 5, 10, and 15 MeV proton irradiation at a fluence of 2.5×10^{14} cm^{-2}.

Irradiation energy (MeV)	R_S ($\Omega/\square$)	R_c (Ω cm^2)
Preirradiation	399	9.39×10^{-6}
5	436	1.14×10^{-5}
10	409	1.03×10^{-5}
15	405	9.80×10^{-6}

cyclotron was 30 MeV. The proton energies at the samples were adjusted to be 5, 10, and 15 MeV by passing through different numbers and thicknesses of aluminum degraders. The irradiated fluence for these three energies was fixed at 2.5×10^{14} cm^{-2}, and the beam currents were measured using a Faraday cup to calculate the flux density.

We used the Stopping and Range of Ions in Matter (SRIM) simulation code to estimate the vacancy density distribution as a function of proton irradiation energy. The gate-lag measurements were conducted with a Hewlett-Packard E3615A power supply, an Agilent 8114A pulse generator, and an Agilent Infinium oscilloscope. The device DC characteristics were measured with an HP 4156 parameter analyzer. Capacitance–voltage values were taken with an Agilent 4284A Precision LCR Meter.

III. RESULTS AND DISCUSSION

Figure 2 shows an SRIM simulation of vacancy concentration as a function of irradiation proton energy. The kinetic energy loss of the protons is a maximum near the end-of-range penetration depths due to the nuclear stopping in that region causing the highest vacancy concentration. The kinetic energy loss of the protons near the wafer surface is dominated by electronic stopping, leading to ionization and sample heating. Although the thickness of wafers investigated is 1000 μm, denoted by the dashed line in Fig. 2(a), the active layer of the MISHEMTs is around 27–30 nm below the surface. The vacancy concentration within the active area of MISHEMT devices was 2 orders of magnitude lower than that near the end-of-range at each proton energy.

FIG. 2. SRIM simulation showing vacancies created within the SiN$_x$/AlGaN/GaN MISHEMTs with respect to proton irradiation energy.
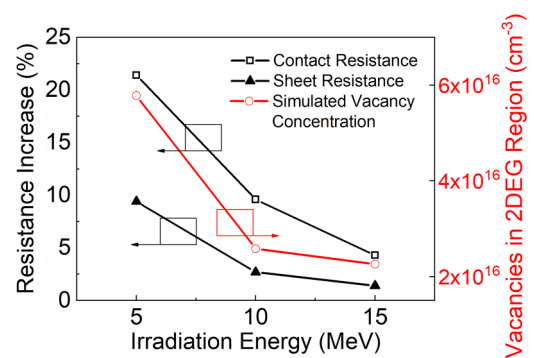

FIG. 3. Sheet and contact resistance increase compared to simulated vacancy concentration in 2DEG region as a function of irradiation energy at a fixed fluence of 2.5×10^{14} cm^{-2}.
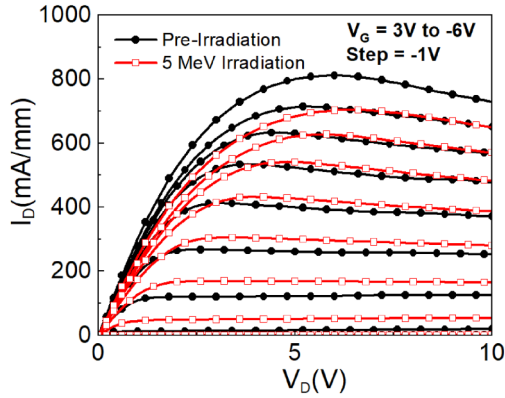
FIG. 4. Drain *I–V* characteristics of the MISHEMT samples irradiated at 5 MeV compared to the samples before irradiation.

TABLE III. Carrier concentration reduction, sheet carrier concentration, and carrier removal rate before and after 5, 10, or 15 MeV proton irradiation at a fluence of 2.5×10^{14} cm^{-2}.

Irradiation energy (MeV)	ΔCarrier concentration reduction (%)	Sheet carrier concentration (cm^{-2})	Carrier removal rate (cm^{-1})
Preirradiation	—	1.26×10^{13}	—
5	9.1	1.13×10^{13}	144
10	2.4	1.21×10^{13}	72
15	0.2	1.24×10^{13}	21

The simulated number of vacancies within the two-dimensional electron gas (2DEG) region of the MISHEMT sample was 5.8×10^{16}, 2.5×10^{16}, and 1.9×10^{16} cm^{-3} for proton energies of 5, 10, and 15 MeV, respectively.

After proton irradiation, no visible degradation of the metallization for either the Ohmic or gate contacts was observed. However, the electrical measurements after proton irradiation indicated notable differences. Table I shows the sheet resistance and contact resistivity measured by the transmission line method (TLM) as a function of proton irradiation energy. The data points shown in Table I represent the mean of eight TLM measurements. After proton irradiation at 15 MeV, the sheet resistance minimally increased from 399 to 405 Ω/□. At irradiation energies of 10 and 5 MeV, the sheet resistance increase was slightly larger, yielding values of 409 and 436 Ω/□, respectively. As shown in Fig. 3, the increase in sheet and contact resistance is consistent with the trend of simulated vacancy concentration within the 2DEG channel. The vacancies generated by proton irradiation result in a greater resistance due to a decreased electron concentration and reduction of the electron mobility. The contact resistance showed a higher degree of degradation compared to the sheet resistance for all proton irradiation energies investigated. At a proton irradiation energy of 5 MeV, a 21% increase of the contact resistance was measured after proton irradiation. The greater degree of degradation in the contact resistance could be caused by annealing damage in the epilayers beneath the Ohmic contacts prior to irradiation. During the high temperature annealing step for Ohmic fabrication, the heterojunction interface reacts with the Ohmic metal causing metal agglomeration and diffusion. These defects induced by annealing are then damaged further by incident protons scattering through the metal at the interface.

Figure 4 shows the drain *I–V* characteristics of the AlGaN/GaN MISHEMT device before and after proton irradiation at 5 MeV and a fluence of 2.5×10^{14} cm^{-2}. The gate was initially biased at 3 V and then stepped down 1 V at a time, while the drain voltage was varied from 0 to 10 V at each respective gate voltage. Table II shows the saturation current reduction and electron mobility reduction as the function of proton irradiation energy. The amount of DC degradation is consistent with the TLM results, with the samples irradiated at 5 MeV showing an average reduction in saturation current of 10.4%. The samples irradiated at 10 MeV had an average current reduction of 3.2%, whereas the samples irradiated at 15 MeV showed saturation current reductions less than 1%. This is a result of less displacement damage near the 2DEG as higher proton energies. The saturation drain current reductions resulted from charged traps in the AlGaN barrier and GaN channel layers. These traps changed the conduction band bending around the 2DEG channel, causing a decreased electron density. As charged traps are generated within the AlGaN and GaN layers, the potential difference between the ground state of subbands (E_0) and the Fermi level (E_F) decreases, causing a change in curvature of the conduction band, resulting in a smaller sheet carrier concentration.[36,37] The displacement damage created within the 2DEG channel results in a lower carrier mobility and reduced carrier density. The low-field linear region of the drain *I–V* curves was used to extract the electron mobility,

TABLE II. Effect of proton irradiation energy on saturation current and electron mobility of AlGaN/GaN MISHEMTs.

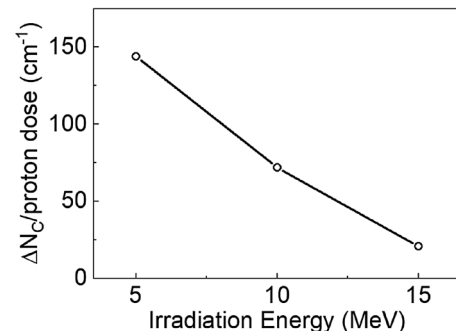| Irradiation energy (MeV)	Saturation I_D reduction (%)	Mobility reduction (%)
5	10.4	25.6
10	3.2	8.1
15	0.5	1.4

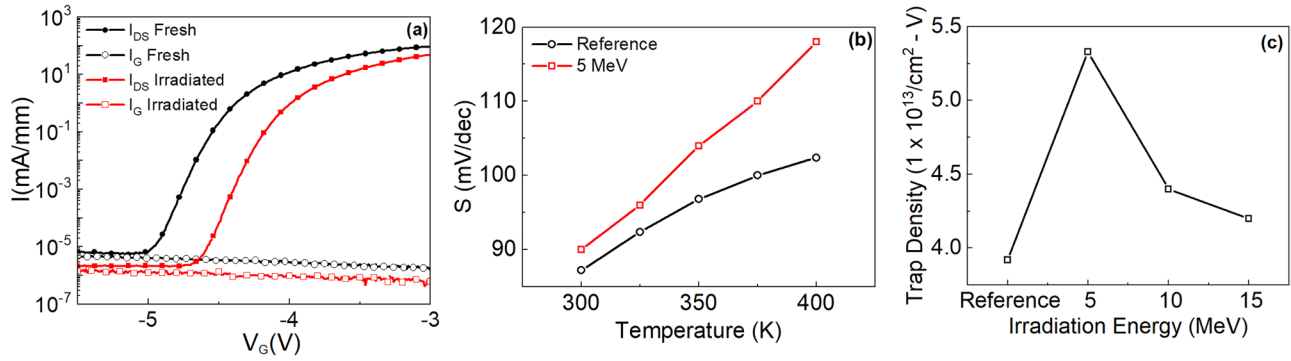FIG. 5. Carrier removal rate as a function of proton irradiation energy.

FIG. 6. (a) Subthreshold characteristics for MISHEMT samples pre- and postirradiation at 5 MeV. (b) Subthreshold swing as a function of temperature before and after irradiation at 5 MeV. (c) Trap density as a function of irradiation energy.

which was calculated using the following equation:

$$\frac{V_{DS}}{I_{DS}} = R_S + R_D + \frac{Ld}{\mu W \varepsilon \varepsilon_0 (V_{GS} - V_{OFF})}, \quad (1)$$

where R_D and R_S are the drain and source resistance, respectively, L is the gate length, ε_0 is the absolute permittivity, ε is the equivalent dielectric constant, d is the equivalent gate dielectric thickness depth of the AlGaN and SiN$_x$ layers, W is the gate width, V_{GS} is the gate voltage, μ is the electron mobility, V_{DS} is the drain voltage, I_{DS} is the drain current, and V_{OFF} is the threshold voltage. There was ~25%, 8%, and 1.5% degradation of carrier mobility for MISHEMT devices irradiated with protons at energies of 5, 10, and 15 MeV, respectively.

Capacitance–voltage measurements were employed to determine the carrier concentration using the following equation:

$$N_D = \frac{2}{q\varepsilon_s \varepsilon_0 A^2 [d(1/C^2)]/dV}, \quad (2)$$

where ε_0 is the absolute permittivity, A is the Schottky area, N_D is the carrier concentration, ε_s is the equivalent dielectric constant, C is the capacitance, q is the elementary charge, and V is the voltage.[38]

Table III displays the carrier concentration reduction, carrier removal rate, and sheet carrier concentration of the proton irradiated MISHEMTs for the three different energies.

The carrier concentration reductions were consistent with the trend of saturation drain current reduction. The carrier removal rate, R$_c$, can be related to the radiation fluence, Φ, initial carrier concentration, n$_o$, and final carrier concentration after irradiation, n, through the following equation:

$$n - n_o = R_c \Phi. \quad (3)$$

This removal rate was calculated using the difference in the sheet carrier concentration before and after the proton irradiation divided by the proton irradiation fluence. Figure 5 shows the carrier removal rate as a function of proton irradiation energy. The carrier removal rate was largest for the devices irradiated at 5 MeV at a value of 144 cm^{-1} compared to the removal rates of 72 and 21 cm^{-1} for the samples irradiated at 10 and 15 MeV, respectively. The carrier removal rate relates the removal of carriers as deep traps are introduced by the radiation. These results provide a practical guide for estimating how much degradation will occur in AlGaN/GaN MISHEMTs for a given fluence of protons.[39]

Figure 6(a) shows the gate and drain currents of the MISHEMTs before and after proton irradiation at an energy of 5 MeV and a fluence of 2.5×10^{14} cm^{-2}. After proton
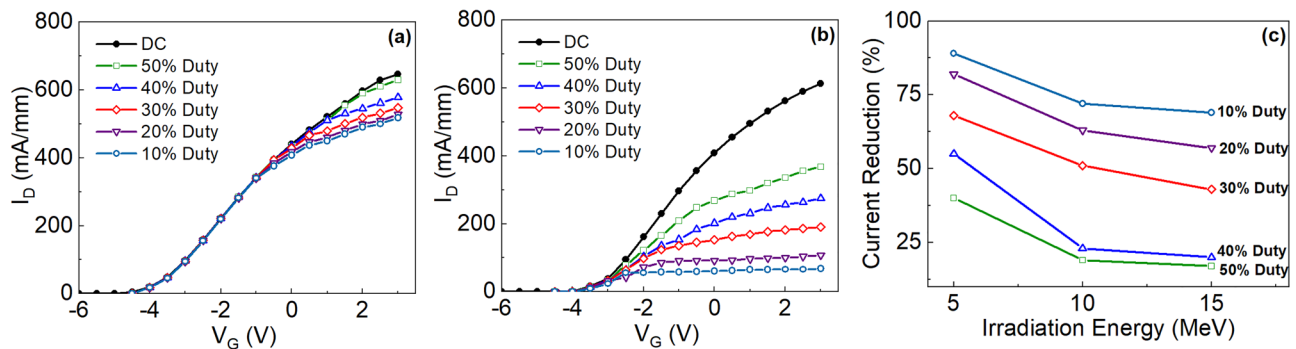

FIG. 7. (a) Gate-lag measurements of MISHEMT sample before proton irradiation as a function of duty cycle. (b) Gate-lag measurements of MISHEMT sample after proton irradiation at an energy of 5 MeV as a function of duty cycle. (c) Gate-lag measurements of MISHEMT samples as a function of irradiation energy and duty cycle.

irradiation, the gate leakage current was reduced by an order of magnitude which was attributed to the irradiated protons reducing the conductivity of the GaN buffer layer therefore improving interdevice isolation. Figure 6(b) illustrates the subthreshold swing of the MISHEMT before and after proton irradiation at an energy of 5 MeV. Subthreshold swing data were measured to identify the trap densities in the gate-modulated region of the MISHEMT devices.[40] Lower subthreshold slope values correspond to lower gate leakage, greater channel control, and a higher device sensitivity. These parameters are necessary for the power efficiency, noise figure, and reliability of power amplifiers. The reference sample exhibited a subthreshold slope of 86 mV/decade, and for the samples irradiated at 10 and 15 MeV, the subthreshold slope remained essentially unchanged compared to the reference. For the samples irradiated at 5 MeV, the subthreshold slope increased slightly to 90 mV/decade indicating that the highest number of proton induced gate traps was generated during the 5 MeV irradiation. This increase is expected because as damage is created within the active regions of the MISHEMTs, the carrier concentration and mobility decrease, causing the device to be less sensitive to gate modulation. The drain current subthreshold swing was measured at temperatures ranging from room temperature to 150 °C before and after proton irradiation. The subthreshold swing is dependent on temperature due to the surface hopping of electrons emitted from the trapped states near the semiconductor/gate interface. The interfacial trap density of the MISHEMT samples can be determined from the change in S as a function of temperature, which can be expressed as

$$D_{it} = \frac{C_{it}}{q}, \tag{4}$$

$$\frac{\partial S}{\partial T} = \frac{k}{q}\left(\ln(10)\left(1 + \frac{C_{it}}{C_{eq}}\right)\right), \tag{5}$$

where D_{it} is the trap density at the interface, q is the magnitude of electronic charges, C_{it} is the interface trap capacitance, S is the subthreshold swing, T is the temperature, k is Boltzmann's constant, and C_{eq} is the equivalent capacitance of the SiN$_x$/GaN/AlGaN layer. Figure 6(c) shows the calculated interface trap density for the MISHEMT samples irradiated at 5, 10, and 15 MeV at a fixed fluence of 2.5×10^{14} cm^{-2}. The MISHEMT interface trap density was largest for the samples irradiated at 5 MeV due to the protons causing a larger degree of lattice damage within the active regions of the devices.

Figure 7(a) illustrates gate-lag measurements performed to determine the result of surface traps of the AlGaN/GaN MISHEMT devices before and after proton irradiation. For this measurement, a constant voltage of 5 V was applied to the drain of the device while the MISHEMT gate was pulsed from −6 V (OFF) to the voltage of interest (ON). The voltage sweep was repeated for duty cycles of 50%–10% using increments of 10 while the pulse rate was kept constant

at 100 kHz. Figure 7(b) depicts the gate-pulsed characteristics compared to the DC current of the MISHEMT devices irradiated at 5 MeV. At lower pulsed gate voltages, nominal degradation was observed to the small voltage differential not yielding hot electrons. When the gate voltage was increased, the large difference between the on-state and off-state of the MISHEMTs generated considerably more hot carriers. Due to the large number of hot carriers, significantly more surface traps become charged and cause a virtual gate to form between the drain and gate of the device. The virtual gate, also referred to as a surface depletion region, yields a lower drain current in the MISHEMT devices which was most pronounced in the samples irradiated at 5 MeV. The drain current relaxation is a consequence of charge trapping and movement in the AlGaN barrier. A qualitative model explains this process by movement of a step of charge trapped on deep states in the barrier and movement of the step toward the interface by multiple emission/capture hops.[40] Figure 7(c) illustrates the effect of proton irradiation energy and duty cycle on the MISHEMT drain current reduction. The current degradation and duty cycle are inversely related. When the duty cycle is lowered, the device is off for a longer fraction of time. At a 10% duty cycle, the device is off for 90% of the pulse period and on for 10% of the pulse period. In the off-state, the large voltage differential causes a significant quantity of hot carriers to travel to dangling bonds on the surface of the MISHEMT. When the duty cycle is increased to 50%, the drain current reduction in devices was 40%, 19%, and 17% for MISHEMTs irradiated at 5, 10, and 15 MeV, respectively.

IV. SUMMARY AND CONCLUSIONS

The effects of proton irradiation energy on AlGaN/GaN MISHEMTs with *in situ* SiN$_x$ cap layers were studied for a fixed fluence of 2.5×10^{14} cm^{-2} at proton energies of 5, 10, and 15 MeV. As the irradiation energy decreased, the maximum transconductance, mobility, saturation drain current, sheet carrier concentration, and high-frequency current retention also decreased. Contact resistance, transfer resistance, sheet resistance, and threshold voltage all increased inversely proportional to the proton irradiation energy. All of the SiN$_x$ passivated AlGaN/GaN MISHEMTs were operational after proton irradiation between 5 and 15 MeV and could be pinched off. For applications like military and satellite communication, AlGaN/GaN MISHEMTs show excellent resilience to high energy proton induced device degradation.

ACKNOWLEDGMENTS

[1]X. L. Wang, C. M. Wang, G. X. Hu, J. X. Wang, T. S. Chen, G. Jiao, J. P. Li, Y. P. Zeng, and J. M. Li, Solid-State Electron. **49**, 1387 (2005).

[2]Y. Irokawa *et al.*, Appl. Phys. Lett. **84**, 2919 (2004).

[3]S. J. Pearton, F. Ren, A. P. Zhang, and K. P. Lee, Mater. Sci. Eng. R Rep. **30**, 55 (2000).

[4]S. C. Binari, K. Ikossi, J. A. Roussos, W. Kruppa, Doewon Park, H. B. Dietrich, D. D. Koleske, A. E. Wickenden, and R. L. Henry, IEEE Trans. Electron Devices **48**, 465 (2001).

[5]R. J. Trew, IEEE Microw. **1**, 46 (2000).

[6]S. R. Messenger, E. A. Burke, G. P. Summers, M. A. Xapsos, R. J. Walters, E. M. Jackson, and B. D. Weaver, IEEE Trans. Nucl. Sci. **46**, 1595 (1999).

[7]G. H. Kinchin and R. S. Pease, Rep. Prog. Phys. **18**, 301 (1955).

[8]J. F. Ziegler and J. P. Biersack, *Treatise Heavy-Ion Science*, edited by D.A. Bromley (Springer, Boston, MA, 1985), pp. 93–129.

[9]D. Braäunig and F. Wulf, Radiat. Phys. Chem. **43**, 105 (1994).

[10]A. Mimouni, T. Fernández, J. Rodriguez-Tellez, A. Tazon, H. Baudrand, and M. Boussuis, Electr. Electron. Eng. **2**, 397 (2013).

[11]Y.-S. Lin, Y.-W. Lain, and S. S. H. Hsu, IEEE Electron Device Lett. **31**, 102 (2010).

[12]G. Meneghesso, F. Rampazzo, P. Kordos, G. Verzellesi, and E. Zanoni, IEEE Trans. Electron Devices **53**, 2932 (2006).

[13]G. Meneghesso, G. Verzellesi, F. Danesin, F. Rampazzo, F. Zanon, A. Tazzoli, M. Meneghini, and E. Zanoni, IEEE Trans. Device Mater. Reliab. **8**, 332 (2008).

[14]J. W. Chung, J. C. Roberts, E. L. Piner, and T. Palacios, IEEE Electron Device Lett. **29**, 1196 (2008).

[15]J. Joh and J. A. del Alamo, "Mechanisms for electrical degradation of GaN high-electron mobility transistors," *2006 International Electron Devices Meeting*, San Francisco, CA, 11-13 December 2006, pp. 1–4.

[16]J.-C. Gerbedoen, A. Soltani, M. Mattalah, M. Moreau, P. Thevenin, and J.-C. De Jaeger, Diam. Relat. Mater. **18**, 1039 (2009).

[17]S. Yagi, M. Shimizu, M. Inada, Y. Yamamoto, G. Piao, H. Okumura, Y. Yano, N. Akutsu, and H. Ohashi, Solid-State Electron. **50**, 1057 (2006).

[18]A. Endoh, Y. Yamashita, N. Hirose, K. Hikosaka, T. Matsui, S. Hiyamizu, and T. Mimura, Jpn. J. Appl. Phys. **45**, 3364 (2006).

[19]C. Fares, F. Ren, S. J. Pearton, G. Yang, J. Kim, C.-F. Lo, and J. W. Johnson, J. Vac. Sci. Technol. B **36**, 11206 (2018).

[20]K.-Y. R. Wong *et al.*, "A next generation CMOS-compatible GaN-on-Si transistors for high efficiency energy systems," *2015 IEEE International Electron Devices Meeting (IEDM)*, Washington, DC, 7-9 December 2015 (IEEE, 2015), pp. 9.5.1–9.5.4.

[21]Z. H. Liu, G. I. Ng, S. Arulkumaran, Y. K. T. Maung, K. L. Teo, S. C. Foo, and S. Vicknesh, IEEE Electron Device Lett. **32**, 318 (2011).

[22]B. M. Green, K. K. Chu, E. M. Chumbes, J. A. Smart, J. R. Shealy, and L. F. Eastman, IEEE Electron Device Lett. **21**, 268 (2000).

[23]J. Ma, X. Lu, X. Zhu, T. Huang, H. Jiang, P. Xu, and K. M. Lau, J. Cryst. Growth **414**, 237 (2015).

[24]K. Cheng, S. Degroote, M. Leys, F. Medjdoub, J. Derluyn, B. Sijmus, M. Germain, and G. Borghs, J. Cryst. Growth **315**, 204 (2011).

[25]X. Hu *et al.*, IEEE Trans. Nucl. Sci. **51**, 293 (2004).

[26]L. Liu *et al.*, J. Vac. Sci. Technol. **31**, 022201 (2013).

[27]Xinwen Hu *et al.*, IEEE Trans. Nucl. Sci. **50**, 1791 (2003).

[28]B. Luo *et al.*, J. Electron. Mater. **31**, 437 (2002).

[29]G. Sonia *et al.*, Solid-State Electron. **52**, 1011 (2008).

[30]H.-Y. Kim, J. Kim, S. P. Yun, K. R. Kim, T. J. Anderson, F. Ren, and S. J. Pearton, J. Electrochem. Soc. **155**, H513 (2008).

[31]S. Ahn *et al.*, J. Vac. Sci. Technol. **33**, 051208 (2015).

[32]S. Ahn, B.-J. Kim, Y.-H. Lin, F. Ren, S. J. Pearton, G. Yang, J. Kim, and I. I. Kravchenko, J. Vac. Sci. Technol. **34**, 051202 (2016).

[33]H.-Y. Kim, J. Kim, L. Liu, C.-F. Lo, F. Ren, and S. J. Pearton, J. Vac. Sci. Technol. **30**, 012202 (2012).

[34]C.-F. Lo *et al.*, J. Vac. Sci. Technol. **30**, 041206 (2012).

[35]C. F. Lo, T. S. Kang, L. Liu, C. Y. Chang, S. J. Pearton, I. I. Kravchenko, O. Laboutin, J. W. Johnson, and F. Ren, Appl. Phys. Lett. **97**, 262116 (2010).

[36]T.-S. Kang, F. Ren, B. P. Gila, S. J. Pearton, E. Patrick, D. J. Cheney, M. Law, and M.-L. Zhang, J. Vac. Sci. Technol. **33**, 061202 (2015).

[37]C. Claeys and E. Simoen, *Radiation Effects in Advanced Semiconductor Materials and Devices* (Springer, Berlin, 2002).

[38]H. Arora, D. S. Rawal, and B. K. Sehgal, *Physics of Semiconductor Devices*, edited by Vinod Kumar Jain and Abhishek Verma (Springer, Cham, 2014), pp. 91–93.

[39]A. Y. Polyakov, N. B. Smirnov, I. V. Shchemerov, F. Ren, and S. J. Pearton, ECS J. Solid State Sci. Technol. **6**, S3034 (2017).

[40]L. Liu *et al.*, J. Vac. Sci. Technol. **29**, 060603 (2011).